

Towards Open-World Generation of Stereo Images and Unsupervised Matching

Feng Qiao Zhexiao Xiong Eric Xing Nathan Jacobs
Washington University in St. Louis

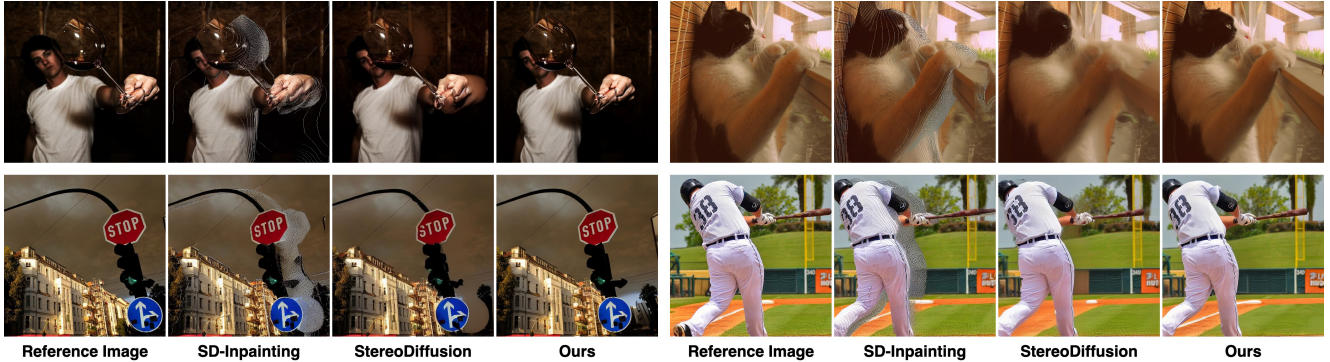


Figure 1. Comparison with diffusion-based methods for stereo image generation on the COCO dataset.

Abstract

Stereo images are fundamental to numerous applications, including extended reality (XR) devices, autonomous driving, and robotics. Unfortunately, acquiring high-quality stereo images remains challenging due to the precise calibration requirements of dual-camera setups and the complexity of obtaining accurate, dense disparity maps. Existing stereo image generation methods typically focus on either visual quality for viewing or geometric accuracy for matching, but not both. We introduce GenStereo, a diffusion-based approach, to bridge this gap. The method includes two primary innovations (1) conditioning the diffusion process on a disparity-aware coordinate embedding and a warped input image, allowing for more precise stereo alignment than previous methods, and (2) an adaptive fusion mechanism that intelligently combines the diffusion-generated image with a warped image, improving both realism and disparity consistency. Through extensive training on 11 diverse stereo datasets, GenStereo demonstrates strong generalization ability. GenStereo achieves state-of-the-art performance in both stereo image generation and unsupervised stereo matching tasks. Project page is available at <https://qjizhi.github.io/genstereo>.

1. Introduction

The demand for stereo images continues growing with XR devices, autonomous driving, and robotics. However, acquiring high-quality stereo images remains chal-

lenging due to complex camera calibration and environmental constraints, limiting the development of robust stereo matching models that generalize well across diverse scenarios. Real-world datasets often provide only sparse disparity annotations [28] or lack accurate ground truth altogether [9]. Although some datasets offer dense, accurate disparity maps [2, 33], they are typically limited to specific scenarios like indoor scenes. Moreover, capturing real-world stereo data requires complex sensor setups with precise calibration, often constraining baseline distances and scene diversity. Synthetic datasets, while providing precise disparity maps, suffer from domain gaps compared to real-world scenarios [5, 56, 57].

Recent advancements in monocular depth estimation (MDE) models [3, 34, 64, 65] have provided increasingly accurate dense disparity maps, playing a crucial role in image generation from single views. Meanwhile, Text-to-Image (T2I) diffusion models, such as Stable Diffusion [35], have made remarkable strides in generating diverse and high-quality images from user-provided text prompts. However, these models often struggle to maintain spatial consistency when altering the viewpoint of the generated images. While there has been some research on 3D novel view generation [38, 53], there remains a gap in utilizing image generation models to directly produce stereo images. StereoDiffusion [55] is the first approach to leverage diffusion-based generation for stereo image generation, but it struggles with pixel-level accuracy, as it applies disparity shifts in the latent space and fills occluded regions with blurry pixels that lack meaningful semantic content. On the other hand, Stable Diffusion Inpainting (SD-

Inpainting) [35], though not designed for stereo image generation, faces similar challenges by incorrectly filling occluded areas with semantically inappropriate pixels. Fig. 1 shows that previous diffusion-based methods and our methods tested on the COCO dataset [23]. The scale factor γ is set to 0.15, meaning that the maximum disparity is 15% of the image width.

We present GenStereo, a novel framework that addresses both visual quality and geometric accuracy in stereo image generation. Existing approaches rely on either warping-based methods [60], which provide geometric accuracy but struggle with semantic consistency in occluded regions, or diffusion-based approaches [55], which maintain better semantic coherence but lack precise geometric control. GenStereo bridges this gap through a carefully designed two-stream architecture inspired by recent advances in human animation [15] and view synthesis [38], achieving both geometric precision and semantic consistency.

Our framework employs a multi-level constraint system for geometric precision and semantic coherence, starting with disparity-aware coordinate embedding that provides implicit geometric guidance. This is followed by a cross-view attention mechanism that enables semantic feature alignment between views, ensuring consistency in challenging areas like occlusions and complex textures. The framework leverages a dual-space supervision strategy that operates in both latent and pixel spaces, with an adaptive fusion mechanism that further optimizes pixel-level accuracy. To ensure robust generalization across diverse real-world scenarios, we train our model on a diverse dataset combining 11 stereo datasets with varying scenes and baselines.

Furthermore, we demonstrate how our high-quality stereo generation framework significantly improves unsupervised stereo matching learning. Previous approaches to unsupervised learning have been limited by either simplified warping and random background filling [60] or constraints to small-scale static scenes [50]. In contrast, our method enables large-scale training with diverse, photorealistic stereo images that maintain both geometric accuracy and semantic consistency. This advancement represents a significant step toward bridging the gap between supervised and unsupervised stereo matching approaches. Our contributions can be summarized as follows:

- We propose GenStereo, the first unified framework for open-world stereo image generation that addresses visual quality and geometric accuracy, enabling both practical applications and unsupervised stereo matching.
- We introduce a comprehensive multi-level constraint system that combines: (1) disparity-aware coordinate embedding with warped image conditioning for geometric guidance, (2) cross-view attention mechanism for semantic feature alignment, and (3) dual-space supervision with adaptive fusion for pixel-accuracy generation.

- Extensive experimental validation demonstrating state-of-the-art performance in both stereo image generation and unsupervised stereo matching.

2. Related Work

2.1. Conditional Diffusion Models

Diffusion models began with DDPM [14], advancing from slow, probabilistic generation to faster sampling with DDIM [41]. Stable Diffusion [35], a pioneering T2I model, further improved efficiency by performing diffusion in a compact latent space, combining it with CLIP-based [32] text conditioning for versatile T2I generation. However, Stable Diffusion lacks fine-grained control over specific visual attributes, relying mainly on text prompts without structured guidance. To address these limitations, conditional diffusion models have emerged. ControlNet [66] is a key advancement, introducing conditioning mechanisms for structural inputs (such as edges, depth maps, or poses) that maintain flexibility while enabling precise, user-driven synthesis. However, ControlNet still faces challenges in achieving pixel-level accuracy in complex images, such as stereo image generation.

Recent research [15, 19, 38, 39, 63] has explored the self-attention properties within T2I models. Text2Video-Zero [19] and MVDream [39] generate consistent visuals across video frames or 3D multi-views by sharing self-attention, while Animate-Anyone [15] and MagicAnimate [63] apply a similar approach to produce human dance videos through fine-tuned T2I models. GenWarp [38] employs augmenting self-attention with cross-view attention between the reference and target views to generate novel images. This two-stream architecture augments the features of the denoising net. Inspired by the adaptability and control of these self-attention-based architectures, our method builds on their strengths. However, their direct application to stereo image generation faces fundamental challenges. First, they typically don't incorporate disparity information, which is crucial for stereoscopic consistency. Second, achieving the pixel-level accuracy required for comfortable stereo viewing demands specialized architectural considerations beyond existing frameworks.

2.2. Stereo Image Generation and Inpainting

Traditional view synthesis approaches, including geometry-based reconstruction [12, 13, 20] and recent NeRF-based methods [50], excel at rendering novel views but are constrained by their requirement for multiple input images of static scenes. While 3D Photography techniques [12, 40] attempt to overcome this limitation through depth-based mesh projection, they often struggle with complex occlusion handling and require sophisticated post-processing pipelines.

The evolution of stereo generation methods has pro-

gressed from simple warping-based approaches to more sophisticated diffusion-based solutions. MfS [60] introduced a basic framework that attempted to handle occlusions by sampling random background patches from the dataset, but this led to semantic inconsistencies and visible artifacts at occlusion areas. While SD-Inpainting [35] introduced more coherent semantic content through its prior learning, it failed to maintain local consistency between inpainted regions and their surrounding context, often producing visible discontinuities in texture and structure. Mono2Stereo [59] made progress by fine-tuning SD-Inpainting specifically for stereo generation, enabling unsupervised stereo matching, though visible artifacts persist in in-painted regions. StereoDiffusion [55] marked a significant shift by introducing end-to-end diffusion-based stereo image generation, but its latent-space warping approach without explicit geometric constraints led to compromised pixel-level accuracy. Despite these advances, the challenge of generating photorealistic stereo images that maintain both visual quality and geometric fidelity remains largely unsolved, particularly for diverse real-world scenarios.

2.3. Unsupervised Stereo Matching

Traditional unsupervised stereo matching approaches primarily rely on photometric consistency. Methods like [11, 47, 48, 67] leverage photometric losses across stereo images, while others [8, 21, 58] extend this to temporal sequences. A parallel line of research explores proxy supervision strategies, either through carefully designed algorithmic supervisors [31, 45, 46] or knowledge distillation from pre-trained networks [1]. Recent domain adaptation approaches [25, 42, 61] attempt to bridge the gap between synthetic and real-world domains or facilitate cross-dataset adaptation. However, these methods often exhibit limited generalization capability beyond their target domains [1], particularly struggling with diverse real-world scenarios.

More recent approaches have explored novel directions for stereo generation and matching. MfS [60] pioneered unsupervised stereo matching using MDE as guidance, but it relies on random background sampling for occlusion filling, leading to semantic inconsistencies. While NeRF-Stereo [50] achieves high-quality results through neural radiance fields, it requires multiple views of static scenes, limiting its practical applications. Mono2Stereo [59] leverages Stable Diffusion for inpainting occluded regions, representing a significant advance in generative stereo synthesis, though it still exhibits artifacts in occluded areas where geometric and semantic consistency is crucial.

3. Methods

Given a left view image I_l and its corresponding disparity map \hat{D}_l predicted by an MDE model, our goal is to generate a high-quality right view image \hat{I}_r that maintains both vi-

sual quality and geometric consistency. As shown in Fig. 2, our GenStereo framework processes the left view as the reference image and synthesizes the right view as the target image. The generated triplet $\langle I_l, \hat{D}_l, \hat{I}_r \rangle$ not only serves as a stereo pair for visualization but also provides training data for unsupervised stereo matching.

3.1. Disparity-Aware Coordinate Embedding

Traditional inpainting-based stereo image generation methods often suffer from visible boundaries between warped and inpainted regions. To address this limitation, we propose a disparity-aware coordinate embedding scheme inspired by recent advances in coordinate-based generation [29, 38]. Our approach utilizes dual coordinate embeddings: a canonical embedding for the left view and its warped counterpart for the right view.

Specifically, we first construct a canonical 2D coordinate map $X \in \mathbb{R}^{h \times w \times 2}$ with values normalized to $[-1, 1]$. This map is transformed into Fourier features [43] through a positional encoding function ϕ :

$$C_l = \phi(X) \quad (1)$$

The resulting Fourier feature map C_l serves as the coordinate embedding for the left view I_l . We then generate the right view embedding by warping C_l according to the disparity map:

$$C_r = \text{warp}(C_l, D_l), \quad (2)$$

where D_l represents ground-truth disparity during training and predicted disparity \hat{D}_l during inference. These coordinate embeddings (C_l and C_r) are integrated into their respective view features (F_l and F_r) through convolutional layers, establishing strong geometric correspondence while maintaining visual consistency between views.

Our approach differs from GenWarp [38] by utilizing disparity maps instead of camera matrices for warping, enabling more precise pixel-level control. We further enhance geometric consistency by incorporating the warped image I_{warp} as additional conditioning for the denoising U-Net.

3.2. Cross-View Feature Enhancement

To facilitate effective information exchange between views, we adopt a two-parallel U-Nets framework pretrained from Stable Diffusion, inspired by GenWarp [38]. However, our work differs in its novel conditioning strategy: the reference U-Net takes concatenated (I_l, C_l) as conditions to process the left view, while the denoising U-Net takes concatenated (I_{warp}, C_r) as conditions when synthesizing the right view \hat{I}_r . This design ensures that each U-Net receives both image content and corresponding coordinate information for better feature extraction. As our model is conditioned on a reference image and its disparity map, we replace text condition of SD with image embedding of the left image through a CLIP image encoder in both U-Nets.

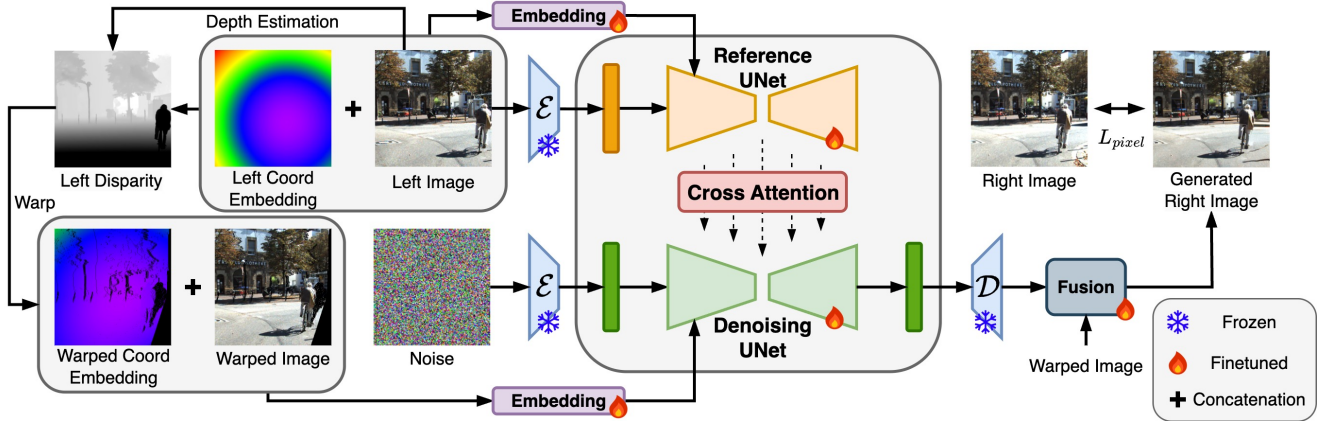


Figure 2. Overview of the GenStereo framework.

To incorporate left-view information during right-view generation, we concatenate the reference features with the target features in the attention mechanism. Specifically, we compute cross-view attention as:

$$q = F_r, \quad k = [F_l, F_r], \quad v = [F_l, F_r]. \quad (3)$$

where F_l is derived from the reference U-Net conditioned on (I_l, C_l) , while F_r comes from the denoising U-Net conditioned on (I_{warp}, C_r) . This dual-stream attention mechanism allows the model to adaptively balance between semantic consistency from the reference view and geometric accuracy from the warped view, with each stream guided by both image content and coordinate information.

3.3. Training Strategy

Mixed training [22, 34, 64] has been proven to be an effective training strategy for domain generalization in both monocular and stereo matching depth estimation. We follow the datasets summarized in [51] and utilize the most widely available public synthetic datasets. Based on our observations, real-world datasets can negatively impact performance, even when there are only minor calibration errors or slight differences in imaging between the two cameras. Tab. 1 shows the comprehensive list of datasets utilized. Datasets containing abstract images are not included, because our model aims to have a good generalization capability in the real world.

To address dataset imbalance, we employ a resampling strategy. Specifically, we sample the smaller datasets multiple times until the number reaches 10% of the largest dataset. As the Stable Diffusion model only accepts images of size 512×512 for SD v1.5 and 768×768 for SD v2.1, we apply a random square crop and resize.

3.4. Pixel Space Alignment

Given an RGB image $I \in \mathbb{R}^{H \times W \times 3}$, Latent Diffusion Models (LDMs) first encode it into a latent representation

Table 1. Our training data sources. All datasets are synthetic with the size of 684K.

Dataset	Indoor	Outdoor	#Images	Year
TartanAir [57]	✓	✓	306K	2020
Dynamic Replica [18]	✓		145K	2023
IRS [56]	✓		103K	2021
Falling Things [52]	✓		61K	2018
VKITTI2 [5]		✓	21K	2020
InfinigenSV [16]		✓	17K	2024
SimStereo [17]		✓	14K	2022
UnrealStereo4K [49]	✓	✓	8K	2021
Spring [27]		✓	5K	2023
PLT-D3 [44]		✓	3K	2024
Sintel [4]		✓	1K	2012

$z = \mathcal{E}(I)$, where $z \in \mathbb{R}^{h \times w \times c}$. While this latent space operation significantly reduces computational costs, it may compromise pixel-level accuracy during image generation.

The standard LDM objective operates in latent space:

$$L_{\text{latent}} := \mathbb{E}_{z, \epsilon, t} [\|\epsilon - \epsilon_{\theta}(z_t, t)\|_2^2] \quad (4)$$

where z_t is the noisy latent at timestep t , ϵ is the noise added to create z_t , and $\epsilon_{\theta}(z_t, t)$ is the network’s prediction of this noise. The model learns to denoise by predicting the noise that was added.

To maintain pixel-level accuracy, we introduce an additional pixel-space loss by decoding both the predicted and target latent variables:

$$L_{\text{pixel}} = \mathbb{E}_{z, \epsilon, t} [\|\mathcal{D}(z_{\text{pred}}) - \mathcal{D}(z_{\text{target}})\|_2^2] \quad (5)$$

The final objective combines both spaces:

$$L = L_{\text{latent}} + \alpha L_{\text{pixel}} \quad (6)$$

where $\alpha = 1$ balances latent and pixel-space supervision.

3.5. Adaptive Fusion Module

To achieve seamless integration between generated and warped content, we propose an Adaptive Fusion Module

that learns to combine I_{gen} and I_{warp} based on local context and confidence. The module predicts spatially-varying fusion weights through a lightweight network:

$$W = \sigma(f_\theta(\text{concat}(I_{gen}, I_{warp}, M))), \quad (7)$$

where f_θ is a 3×3 convolutional layer and σ is the sigmoid activation, ensuring weights in $[0, 1]$. The final right view is computed as:

$$\hat{I}_r = M \odot W \odot I_{warp} + (1 - M \odot W) \odot I_{gen}, \quad (8)$$

where \odot denotes element-wise multiplication. This formulation adaptively favors warped content in high-confidence regions ($M \approx 1$) while relying on generated content in occluded or uncertain areas. The learned weights W enable smooth transitions between warped and generated regions, ensuring both geometric accuracy and visual consistency.

3.6. Random Disparity Dropout

To simulate the sparsity of real-world disparity maps like KITTI’s LiDAR-derived ground truth, we randomly apply disparity dropout to 10% of training samples. For each selected sample, we first generate a dropout ratio:

$$r \sim \text{Uniform}(0, 1) \quad (9)$$

Using this ratio, we create a binary mask where each pixel has a probability r of being dropped:

$$M_{\text{rand}}(i, j) = \begin{cases} 1 & \text{otherwise} \\ 0 & \text{with probability } r \end{cases} \quad (10)$$

The final mask combines this random dropout with the warping mask:

$$M = M_{\text{warp}} \vee M_{\text{rand}} \quad (11)$$

where \vee denotes element-wise logical OR. This strategy encourages the model to handle sparse disparity inputs, improving its robustness and generalization to real-world scenarios where dense disparity maps may not be available.

4. Experiments

4.1. Stereo Image Generation

Experimental Setup. We fine-tune the pretrained Stable Diffusion (SD) UNet for 3 epochs across all experiments. For evaluation, we utilize two widely adopted stereo vision benchmarks: Middlebury 2014 [36] and KITTI 2015 [28], neither of which are included in our training set. Middlebury 2014 comprises 23 high-resolution indoor stereo pairs captured with wide-baseline stereo cameras under varying illumination conditions, providing challenging scenarios for stereo generation. KITTI 2015 contains 200 outdoor stereo

pairs of street scenes with LiDAR-based sparse disparity ground truth, offering diverse real-world testing scenarios. Following StereoDiffusion [55], we preprocess Middlebury images to 512×512 resolution, while KITTI images are center-cropped before resizing to 512×512 to maintain the most informative regions.

We conduct comprehensive comparisons against both traditional and learning-based baselines. Traditional approaches include naïve solutions such as leave blank and image stretching. For learning-based comparisons, we evaluate against state-of-the-art diffusion models adapted for stereo generation: Repaint [26] and SD-Inpainting [35], as well as StereoDiffusion, which specifically targets stereo image generation. To quantitatively assess the quality of generated right-view images (\hat{I}_r) against ground truth (I_r), we employ three complementary metrics: Peak Signal-to-Noise Ratio (PSNR), Structural Similarity Index Measure (SSIM), and Learned Perceptual Image Patch Similarity (LPIPS) with SqueezeNet backbone.

Quantitative Results. Tab. 2 presents the generation performance on Middlebury 2014 and KITTI 2015. The sparsity of ground truth disparities in KITTI limits evaluation accuracy, making pseudo-label disparities more effective for assessing stereo consistency. This sparsity particularly affects inpainting-based methods, as they struggle to infer accurate right-view images in areas with missing depth information, especially for dynamic objects and distant regions. In contrast, Middlebury 2014, which provides dense ground truth disparities, demonstrates a smaller performance gap between using ground truth and using pseudo disparities, underscoring the advantage of high-quality disparity annotations for generation. We obtain pseudo disparities from CREStereo [22] pretrained model, where evaluation datasets are not used for training.

Qualitative Results. We present qualitative comparisons between our method and several baselines: leave blank, StereoDiffusion, and SD-Inpainting, with ground truth as reference. As shown in Fig. 3, our method demonstrates superior performance on the Middlebury 2014 dataset. While SD-Inpainting struggles with occlusion handling, often generating semantically inconsistent content in occluded regions, and StereoDiffusion exhibits loss of fine details due to latent-space warping, our approach successfully maintains both geometric accuracy and visual fidelity. Particularly noteworthy is our method’s ability to generate coherent right-view images while preserving pixel-level correspondence with the left images. Additional qualitative results on the KITTI 2015 dataset and more visualizations on other datasets can be found in the supplementary materials.

4.2. Unsupervised Learning

Experimental Setup. We conduct two comprehensive experiments to validate the effectiveness of our proposed gen-

Table 2. Quantitative results of image generation for Middlebury 2014 and KITTI 2015 datasets. The top three results for each metric are highlighted with a **first**, **second**, and **third** background, respectively.

Methods	SD version	Middlebury 2014			KITTI 2015		
		PSNR \uparrow	SSIM \uparrow	LPIPS \downarrow	PSNR \uparrow	SSIM \uparrow	LPIPS \downarrow
Leave blank	-	11.328 ^{+2.483} -3.489	0.315 ^{+0.230} -0.154	0.450 ^{+0.097} -0.089	12.980 ^{+4.919} -3.831	0.374 ^{+0.286} -0.251	0.313 ^{+0.222} -0.109
Stretch	-	14.842 ^{+2.714} -2.753	0.432 ^{+0.190} +0.265	0.285 ^{+0.112} -0.089	14.757 ^{+5.375} -4.694	0.429 ^{+0.287} -0.271	0.212 ^{+0.145} -0.100
3D Photography [40]	-	14.190 ^{+2.464} -2.798	0.427 ^{+0.175} -0.238	0.275 ^{+0.073} -0.065	14.540 ^{+7.256} -4.023	0.398 ^{+0.270} -0.323	0.210 ^{+0.099} -0.073
RePaint [26]	1.5	15.102 ^{+2.909} -2.802	0.462 ^{+0.268} -0.253	0.311 ^{+0.088} -0.079	15.056 ^{+5.366} -4.897	0.462 ^{+0.268} -0.285	0.251 ^{+0.128} -0.095
SD-Inpainting [35]	1.5	15.740 ^{+3.511} -3.351	0.412 ^{+0.188} -0.236	0.311 ^{+0.164} -0.098	9.792 ^{+2.809} -4.070	0.230 ^{+0.229} +0.236	0.652 ^{+0.144} -0.139
StereoDiffusion [55]	1.5	15.456 ^{+2.669} -3.313	0.468 ^{+0.252} -0.205	0.231 ^{+0.096} -0.088	15.679 ^{+5.888} -5.487	0.481 ^{+0.245} -0.310	0.205 ^{+0.135} -0.099
Ours + GT	1.5	23.699 ^{+5.456} -6.033	0.866 ^{+0.084} -0.141	0.064 ^{+0.053} -0.034	20.439 ^{+7.518} -8.541	0.746 ^{+0.155} -0.274	0.108 ^{+0.117} -0.048
Ours + Pseudo	1.5	23.835 ^{+6.842} -6.741	0.868 ^{+0.096} -0.157	0.062 ^{+0.063} -0.038	22.749 ^{+6.722} -6.102	0.813 ^{+0.110} -0.152	0.096 ^{+0.068} -0.040
Ours + GT	2.1	24.819 ^{+4.519} -4.252	0.906 ^{+0.057} -0.132	0.061 ^{+0.059} -0.032	19.836 ^{+8.952} -8.483	0.765 ^{+0.137} -0.245	0.135 ^{+0.104} -0.059
Ours + Pseudo	2.1	25.142 ^{+6.970} -4.872	0.911 ^{+0.066} -0.133	0.060 ^{+0.061} -0.037	23.488 ^{+7.090} -6.444	0.849 ^{+0.092} -0.130	0.109 ^{+0.068} -0.050

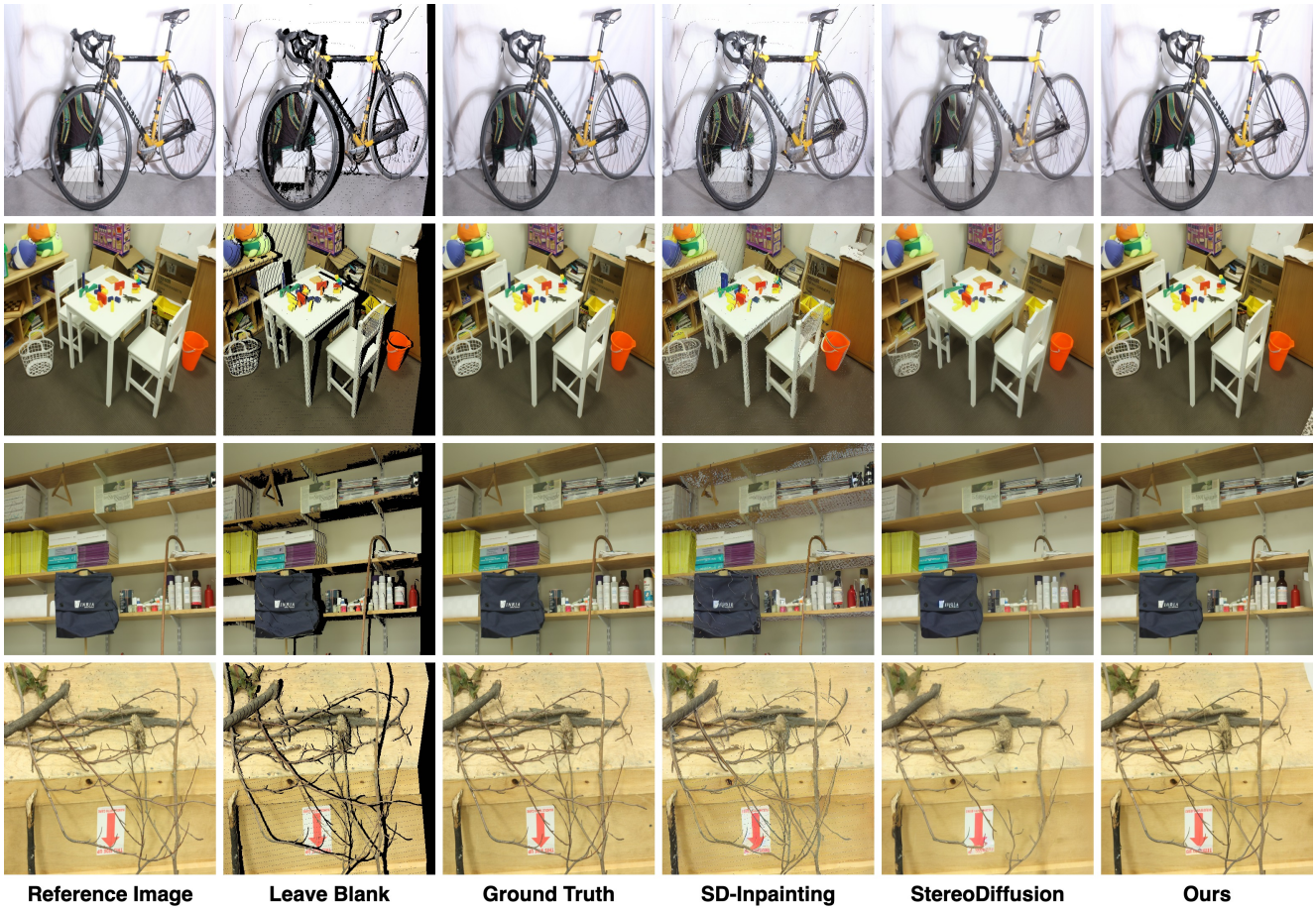


Figure 3. Qualitative comparison on Middlebury 2014 with ground truth disparity maps.

eration method for unsupervised stereo matching.

In the first experiment, we fine-tune a stereo matching model pretrained on the SceneFlow dataset using the KITTI 2012 and KITTI 2015 benchmarks. We split the training and evaluation sets into 160/34 images for KITTI 2012 and 160/40 images for KITTI 2015, following [60].

The second experiment evaluates various unsupervised

stereo matching approaches by generating stereo images. Specifically, KITTI 2012 [10] has 194 stereo images, KITTI 2015 has 200 stereo images, ETH3D [37] has 27 stereo pairs, and the Middlebury v3 training set [36] has 15 stereo pairs at Quarter and Half resolutions (Mid-Q, Mid-H). This diverse dataset selection allows us to comprehensively assess the generalization capability of our method across

Table 3. Comparison with other diffusion-based stereo image generation methods for unsupervised stereo matching. The first group of methods is trained on PSMNet while the second group is trained on RAFT-Stereo. SD v1.5 is used for the experiments.

Methods	KITTI 2012		KITTI 2015	
	D1-all ↓	EPE ↓	D1-all ↓	EPE ↓
Leave blank	25.219	3.542	24.568	2.937
SD-Inpainting [35]	3.907	0.894	4.490	1.059
StereoDiffusion [55]	15.213	2.220	5.651	1.154
Ours	3.802	0.815	3.933	0.991
Leave blank	4.184	0.952	4.074	0.957
SD-Inpainting [35]	4.016	0.945	4.128	0.972
StereoDiffusion [55]	12.756	1.811	6.360	1.174
Ours	3.537	0.930	3.653	0.943

different domains and resolutions.

We evaluate the performance of various unsupervised stereo matching approaches using the D1-all metric, which measures the percentage of incorrect disparity predictions (error $> 3\text{px}$ or 5% of the true disparity), the End-Point-Error (EPE), and the $>n\text{px}$ metric, which denotes the percentage of pixels with an EPE exceeding n pixels. To demonstrate the architecture-agnostic nature of our approach, we employ three distinct stereo models: PSMNet [6], a cost-volume-based method, RAFT-Stereo [24], an iterative refinement model, and IGEV++ [62], one of the most recent methods. For disparity estimation, we utilize the Depth Anything Model v2 (DAMv2) [65], from which we obtain the disparity map. The disparity values are normalized to the range $[0, 1]$ and subsequently scaled by a factor γ to enable flexibility generation.

Fine-tuning on KITTI. To ensure fair and consistent comparisons across all generation methods, we construct the training datasets using a standardized procedure. Specifically, we sample the scale factor γ from the set $\{0.05, 0.1, 0.15, 0.2, 0.25\}$. For each selected scale, we employ various generation methods to create the right images based on 160 left images and their corresponding scaled disparity maps for both KITTI 2012 and KITTI 2015. This procedure results in a total of 800 stereo pairs.

As shown in Tab. 3, higher generation quality leads to improved stereo matching performance. Among the compared methods, SD-Inpainting achieves the closest performance to ours due to its pixel-level warping operation. However, it falls short in providing semantic consistency in occluded areas, which limits its overall effectiveness.

Unsupervised Generalization. Following the methodology of constructing the Mono for Stereo (MfS) dataset in [60], we construct our training dataset, MfS-GenStereo, from the same datasets, including ADE20K [68], Mapillary Vistas [30], DIODE [54], Depth in the Wild [7], and COCO 2017 [23]. During the generation process, we randomly select a scale factor in the range $[0, 0.35]$ and set the maxi-

imum disparity to 256 for PSMNet. As shown in Tab. 4, our method enables unsupervised stereo matching using only left images, achieving superior performance.

We compare our approach with the original MfS [60] and its enhanced variant using the Depth Anything Model v2 (DAMv2), which generates the right view images by filling the occluded areas with random background patches from the dataset. The experiments indicate that, despite the better depth prior, the synthesis of right-view images remains a critical bottleneck in this methodology. Additionally, we compare with Mono2Stereo, which fine-tunes SD-Inpainting for right-view image generation, and NeRF-Stereo, which generates stereo images by reconstructing the static scenes using Neural Radiance Fields (NeRF), limiting the diversity of its datasets. Our experimental results indicate that our proposed method consistently surpasses these existing approaches in generating high-quality stereo pairs with pixel-level accuracy, demonstrating robust generalization capabilities and significantly enhancing stereo matching performance across diverse datasets.

4.3. Ablation Study.

Random disparity drop. Since the ground-truth disparity maps in real-world datasets (e.g., KITTI) are often derived from LiDAR, resulting in sparse and incomplete point clouds, our random disparity dropout strategy mitigates the model’s reliance on dense disparity supervision. This enhancement allows the model to generate plausible right images even when only sparse disparity maps are available. This strategy significantly improves performance on datasets with sparse ground-truth annotations, demonstrating better generalization to real-world scenarios. As shown in Tab. 5, comparing rows (1) and (2) highlights the effectiveness of this strategy.

Mixed datasets. We train our model on Virtual KITTI 2 (VKITTI2) [5] and a combination of mixed datasets, and subsequently evaluate both models. When trained exclusively on VKITTI2, the model achieves comparable performance to the mixed-dataset model on KITTI 2015, owing to the relatively small domain gap between VKITTI2 and KITTI 2015. However, this single-dataset training results in notable performance degradation on other datasets, indicating limited generalization. As shown in Tab. 5, comparing rows (3) and (8) demonstrates that our mixed dataset training strategy significantly improves the model’s generalization across diverse domains.

Coordinate embedding and the warped image. Incorporating the coordinate embedding process effectively encodes spatial information and reinforces the structural relationship between stereo views. Additionally, using the warped image as a condition enhances performance by providing pixel-level guidance. The warped image serves as a coarse prediction of the right view, helping the model focus

Table 4. Zero-Shot Generalization Benchmark. The first group shows methods trained with PSMNet, the second group shows methods trained with RAFT-Stereo, and the third group represents IGEV++.

Methods	KITTI 2012			KITTI 2015			ETH3D			Middlebury-Q			Middlebury-H		
	D1-all	EPE	>3px	D1-all	EPE	>3px	D1-all	EPE	>1px	D1-all	EPE	>2px	D1-all	EPE	>2px
PSMNet [6]	26.69	3.877	27.35	28.24	4.003	28.53	4.258	1.989	15.74	15.00	4.941	20.20	21.34	9.899	33.26
MfS [60]	4.322	1.009	4.703	4.963	1.636	5.181	2.204	0.535	8.170	9.217	1.648	12.07	12.34	3.242	17.56
MfS+DAMv2 [65]	4.931	1.063	5.313	5.504	1.401	5.737	1.990	0.493	8.145	9.447	1.825	11.90	12.34	3.678	17.21
Mono2Stereo [59]	4.077	0.859	-	4.507	1.052	-	1.531	0.397	-	-	-	-	-	-	-
NeRFStereo [50]	3.683	0.851	4.507	4.813	1.448	5.041	1.620	0.557	11.68	7.619	1.451	11.04	8.892	2.590	12.88
Ours + SD v1.5	3.676	0.846	4.063	3.879	0.996	4.112	1.114	0.378	5.556	6.887	1.139	10.43	11.33	2.269	19.39
Ours + SD v2.1	3.807	0.820	4.122	3.898	0.978	4.096	0.894	0.324	4.101	5.037	0.860	7.463	8.046	1.709	13.73
RAFT-Stereo [24]	3.944	0.830	4.239	5.254	1.132	5.468	0.883	0.267	2.607	5.157	1.217	10.25	5.774	1.436	11.20
NeRFStereo [50]	3.787	0.855	4.140	5.356	1.469	5.561	0.830	0.301	3.370	5.819	1.003	8.370	7.426	1.820	10.95
Ours + SD v1.5	3.224	0.734	3.455	4.683	1.042	4.897	0.959	0.294	2.667	3.450	1.003	7.952	4.446	1.514	9.94
Ours + SD v2.1	3.219	0.716	3.019	3.950	0.971	4.222	0.835	0.277	2.638	4.067	1.127	9.382	4.618	1.527	11.11
IGEV++ [62]	5.681	1.099	6.196	6.028	1.265	6.239	1.701	0.356	4.666	4.238	0.828	6.274	5.292	2.384	7.752
Ours + SD v2.1	2.802	0.686	3.015	3.746	0.952	4.004	1.226	0.326	3.429	3.682	0.684	5.512	2.797	0.842	5.098

Table 5. Ablation studies. SD v1.5 is used for the experiments.

Disparity Source	#	Mixed Datasets	Random Drop	Coord Embedding	Warped Image	Pixel Loss	Fusion	Middlebury 2014			KITTI 2015		
								PSNR	SSIM	LPIPS	PSNR	SSIM	LPIPS
Ground Truth	(1)	✓	✗	✓	✓	✓	✓	23.552	0.862	0.0641	16.164	0.664	0.1740
	(2)	✓	✓	✓	✓	✓	✓	23.699	0.866	0.0635	20.439	0.746	0.1079
Pseudo Disparities	(3)	✗	✓	✓	✓	✓	✓	20.037	0.745	0.1214	21.085	0.777	0.1113
	(4)	✓	✓	✓	✗	✗	✗	22.033	0.796	0.0731	21.866	0.779	0.1002
	(5)	✓	✓	✗	✓	✗	✗	22.697	0.832	0.0715	22.313	0.798	0.1011
	(6)	✓	✓	✓	✓	✗	✗	23.407	0.855	0.0644	22.520	0.805	0.0974
	(7)	✓	✓	✓	✓	✓	✗	23.811	0.867	0.0621	22.716	0.811	0.0961
	(8)	✓	✓	✓	✓	✓	✓	23.835	0.868	0.0620	22.749	0.813	0.0958

on correcting local inconsistencies rather than synthesizing the entire image from scratch. As shown in rows (4), (5), and (6) in Tab. 5, the combination of coordinate embedding and warped image significantly improves generation performance, preserving geometric consistency and reducing artifacts like stitching boundaries. While warped image embedding contributes most to performance, its effectiveness decreases with additional fine-tuning iterations, revealing instability when using warped image alone as a conditioning signal. This underscores the importance of combining coordinate embedding and warped image to achieve stable, high-quality stereo image generation.

Pixel-level loss. By decoding the latent representations back to the image space, the model learns to minimize discrepancies directly in the observed image space, enforcing pixel-level alignment. As illustrated in rows (6) and (7), the introduction of the pixel-level loss significantly improves the generation performance, highlighting its role in maintaining high-fidelity stereo image generation.

Adaptive Fusion. The proposed adaptive fusion module significantly enhances visual quality by dynamically weighting the contributions of both the generated and warped images. A comparison of rows (7) and (8) demonstrates that this fusion strategy further refines pixel alignment, resulting in sharper, more structurally coherent, and

perceptually accurate reconstructions. The improvement in PSNR is more pronounced than that in SSIM and LPIPS, indicating that the adaptive fusion is particularly effective for pixel-level alignment.

5. Conclusion

We presented GenStereo, a novel diffusion-based framework for open-world stereo image generation with applications in unsupervised stereo matching. Our method introduces several key innovations, including disparity-aware coordinate embeddings along with warped image embeddings, pixel-level loss, and an adaptive fusion module, to ensure high-quality stereo image generation with strong geometric and semantic consistency. Through extensive experiments across diverse datasets, we show that GenStereo significantly outperforms existing methods in both stereo generation and unsupervised matching. Our ablation studies demonstrate the efficacy of each proposed component.

Limitations. Despite promising results, diffusion-based models face inherent challenges with large disparities when generating right-view images due to large unconditioned regions. While our data augmentation such as random cropping and resizing mitigates these issues and performs well in typical stereo setups, future work could explore extending these models to accommodate larger disparities.

Acknowledgments

We gratefully acknowledge the advanced computational resources provided by Engineering IT and Research Infrastructure Services at Washington University in St. Louis.

References

- [1] Filippo Aleotti, Fabio Tosi, Li Zhang, Matteo Poggi, and Stefano Mattoccia. Reversing the cycle: self-supervised deep stereo through enhanced monocular distillation. In *European Conference on Computer Vision*, pages 614–632. Springer, 2020. 3
- [2] Wei Bao, Wei Wang, Yuhua Xu, Yulan Guo, Siyu Hong, and Xiaohu Zhang. Instereo2k: a large real dataset for stereo matching in indoor scenes. *Science China Information Sciences*, 63:1–11, 2020. 1
- [3] Shariq Farooq Bhat, Reiner Birkel, Diana Wofk, Peter Wonka, and Matthias Müller. Zoedepth: Zero-shot transfer by combining relative and metric depth. *arXiv preprint arXiv:2302.12288*, 2023. 1
- [4] D. J. Butler, J. Wulff, G. B. Stanley, and M. J. Black. A naturalistic open source movie for optical flow evaluation. In *European Conf. on Computer Vision*, pages 611–625. Springer-Verlag, 2012. 4
- [5] Yohann Cabon, Naila Murray, and Martin Humenberger. Virtual kitti 2. *arXiv preprint arXiv:2001.10773*, 2020. 1, 4, 7
- [6] Jia-Ren Chang and Yong-Sheng Chen. Pyramid stereo matching network. In *IEEE Conference on Computer Vision and Pattern Recognition*, pages 5410–5418, 2018. 7, 8
- [7] Weifeng Chen, Zhao Fu, Dawei Yang, and Jia Deng. Single-image depth perception in the wild. *Advances in neural information processing systems*, 29, 2016. 7
- [8] Cheng Chi, Qingjie Wang, Tianyu Hao, Peng Guo, and Xin Yang. Feature-level collaboration: Joint unsupervised learning of optical flow, stereo depth and camera motion. In *IEEE/CVF Conference on Computer Vision and Pattern Recognition*, pages 2463–2473, 2021. 3
- [9] Jaehoon Cho, Dongbo Min, Youngjung Kim, and Kwanghoon Sohn. Deep monocular depth estimation leveraging a large-scale outdoor stereo dataset. *Expert Systems with Applications*, 178:114877, 2021. 1
- [10] Andreas Geiger, Philip Lenz, and Raquel Urtasun. Are we ready for autonomous driving? the kitti vision benchmark suite. In *2012 IEEE Conference on Computer Vision and Pattern Recognition*, pages 3354–3361. IEEE, 2012. 6
- [11] Clément Godard, Oisín Mac Aodha, Michael Firman, and Gabriel J Brostow. Digging into self-supervised monocular depth estimation. In *IEEE/CVF international conference on computer vision*, pages 3828–3838, 2019. 3
- [12] Peter Hedman, Suhil Alsian, Richard Szeliski, and Johannes Kopf. Casual 3d photography. *ACM Transactions on Graphics (TOG)*, 36(6):1–15, 2017. 2
- [13] Peter Hedman, Julien Philip, True Price, Jan-Michael Frahm, George Drettakis, and Gabriel Brostow. Deep blending for free-viewpoint image-based rendering. *ACM Transactions on Graphics (TOG)*, 37(6):1–15, 2018. 2
- [14] Jonathan Ho, Ajay Jain, and Pieter Abbeel. Denoising diffusion probabilistic models. *Advances in neural information processing systems*, 33:6840–6851, 2020. 2
- [15] Li Hu. Animate anyone: Consistent and controllable image-to-video synthesis for character animation. In *IEEE/CVF Conference on Computer Vision and Pattern Recognition*, pages 8153–8163, 2024. 2
- [16] Junpeng Jing, Ye Mao, and Krystian Mikolajczyk. Match-stereo-videos: Bidirectional alignment for consistent dynamic stereo matching. In *European Conference on Computer Vision*, pages 415–432. Springer, 2024. 4
- [17] Laurent Valentin Jospin, Hamid Laga, Farid Boussaid, and Mohammed Bennamoun. Active-passive simstereo, 2022. 4
- [18] Nikita Karaev, Ignacio Rocco, Benjamin Graham, Natalia Neverova, Andrea Vedaldi, and Christian Ruppert. Dynamicstereo: Consistent dynamic depth from stereo videos. In *IEEE/CVF Conference on Computer Vision and Pattern Recognition*, pages 13229–13239, 2023. 4
- [19] Levon Khachatryan, Andranik Movsisyan, Vahram Tadevosyan, Roberto Henschel, Zhangyang Wang, Shant Navasardyan, and Humphrey Shi. Text2video-zero: Text-to-image diffusion models are zero-shot video generators. In *IEEE/CVF International Conference on Computer Vision*, pages 15954–15964, 2023. 2
- [20] Johannes Kopf, Fabian Langguth, Daniel Scharstein, Richard Szeliski, and Michael Goesele. Image-based rendering in the gradient domain. *ACM Transactions on Graphics (TOG)*, 32(6):1–9, 2013. 2
- [21] Hsueh-Ying Lai, Yi-Hsuan Tsai, and Wei-Chen Chiu. Bridging stereo matching and optical flow via spatiotemporal correspondence. In *IEEE/CVF Conference on Computer Vision and Pattern Recognition*, pages 1890–1899, 2019. 3
- [22] Jiankun Li, Peisen Wang, Pengfei Xiong, Tao Cai, Ziwei Yan, Lei Yang, Jiangyu Liu, Haoqiang Fan, and Shuaicheng Liu. Practical stereo matching via cascaded recurrent network with adaptive correlation. In *IEEE/CVF Conference on Computer Vision and Pattern Recognition*, pages 16263–16272, 2022. 4, 5
- [23] Tsung-Yi Lin, Michael Maire, Serge Belongie, James Hays, Pietro Perona, Deva Ramanan, Piotr Dollár, and C Lawrence Zitnick. Microsoft coco: Common objects in context. In *European Conference on Computer Vision*, pages 740–755. Springer, 2014. 2, 7
- [24] Lahav Lipson, Zachary Teed, and Jia Deng. Raft-stereo: Multilevel recurrent field transforms for stereo matching. In *IEEE International Conference on 3D Vision*, pages 218–227, 2021. 7, 8
- [25] Rui Liu, Chengxi Yang, Wenxiu Sun, Xiaogang Wang, and Hongsheng Li. Stereogan: Bridging synthetic-to-real domain gap by joint optimization of domain translation and stereo matching. In *IEEE/CVF Conference on Computer Vision and Pattern Recognition*, pages 12757–12766, 2020. 3
- [26] Andreas Lugmayr, Martin Danelljan, Andres Romero, Fisher Yu, Radu Timofte, and Luc Van Gool. Repaint: Inpainting using denoising diffusion probabilistic models. In *IEEE/CVF Conference on Computer Vision and Pattern Recognition*, pages 11461–11471, 2022. 5, 6

- [27] Lukas Mehl, Jenny Schmalfluss, Azin Jahedi, Yaroslava Naliyayko, and Andrés Bruhn. Spring: A high-resolution high-detail dataset and benchmark for scene flow, optical flow and stereo. In *IEEE/CVF Conference on Computer Vision and Pattern Recognition*, 2023. 4
- [28] Moritz Menze and Andreas Geiger. Object scene flow for autonomous vehicles. In *IEEE Conference on Computer Vision and Pattern Recognition*, pages 3061–3070, 2015. 1, 5
- [29] Jiteng Mu, Shalini De Mello, Zhiding Yu, Nuno Vasconcelos, Xiaolong Wang, Jan Kautz, and Sifei Liu. Coordgan: Self-supervised dense correspondences emerge from gans. In *IEEE/CVF Conference on Computer Vision and Pattern Recognition*, pages 10011–10020, 2022. 3
- [30] Gerhard Neuhof, Tobias Ollmann, Samuel Rota Buló, and Peter Kotschieder. The mapillary vistas dataset for semantic understanding of street scenes. In *IEEE international conference on computer vision*, pages 4990–4999, 2017. 7
- [31] Matteo Poggi, Alessio Tonioni, Fabio Tosi, Stefano Mattoccia, and Luigi Di Stefano. Continual adaptation for deep stereo. *IEEE Transactions on Pattern Analysis and Machine Intelligence*, 44(9):4713–4729, 2021. 3
- [32] Alec Radford, Jong Wook Kim, Chris Hallacy, Aditya Ramesh, Gabriel Goh, Sandhini Agarwal, Girish Sastry, Amanda Askell, Pamela Mishkin, Jack Clark, et al. Learning transferable visual models from natural language supervision. In *International conference on machine learning*, pages 8748–8763. PMLR, 2021. 2
- [33] Pierluigi Zama Ramirez, Alex Costanzino, Fabio Tosi, Matteo Poggi, Samuele Salti, Stefano Mattoccia, and Luigi Di Stefano. Booster: a benchmark for depth from images of specular and transparent surfaces. *IEEE Transactions on Pattern Analysis and Machine Intelligence*, 2023. 1
- [34] René Ranftl, Katrin Lasinger, David Hafner, Konrad Schindler, and Vladlen Koltun. Towards robust monocular depth estimation: Mixing datasets for zero-shot cross-dataset transfer. *IEEE transactions on pattern analysis and machine intelligence*, 44(3):1623–1637, 2020. 1, 4
- [35] Robin Rombach, Andreas Blattmann, Dominik Lorenz, Patrick Esser, and Björn Ommer. High-resolution image synthesis with latent diffusion models. In *IEEE/CVF Conference on Computer Vision and Pattern Recognition*, pages 10684–10695, 2022. 1, 2, 3, 5, 6, 7
- [36] Daniel Scharstein, Heiko Hirschmüller, York Kitajima, Greg Krathwohl, Nera Nešić, Xi Wang, and Porter Westling. High-resolution stereo datasets with subpixel-accurate ground truth. In *Pattern Recognition: 36th German Conference, GCPR 2014, Münster, Germany, September 2-5, 2014, Proceedings 36*, pages 31–42. Springer, 2014. 5, 6
- [37] Thomas Schops, Johannes L Schonberger, Silvano Galliani, Torsten Sattler, Konrad Schindler, Marc Pollefeys, and Andreas Geiger. A multi-view stereo benchmark with high-resolution images and multi-camera videos. In *IEEE Conference on Computer Vision and Pattern Recognition*, pages 3260–3269, 2017. 6
- [38] Junyoung Seo, Kazumi Fukuda, Takashi Shibuya, Takuya Narihira, Naoki Murata, Shoukang Hu, Chieh-Hsin Lai, Seungryong Kim, and Yuki Mitsufuji. Genwarp: Single image to novel views with semantic-preserving generative warping. *Advances in Neural Information Processing Systems (NeurIPS)*, 2024. 1, 2, 3
- [39] Yichun Shi, Peng Wang, Jianglong Ye, Mai Long, Kejie Li, and Xiao Yang. Mvdream: Multi-view diffusion for 3d generation. *arXiv preprint arXiv:2308.16512*, 2023. 2
- [40] Meng-Li Shih, Shih-Yang Su, Johannes Kopf, and Jia-Bin Huang. 3d photography using context-aware layered depth inpainting. In *IEEE/CVF Conference on Computer Vision and Pattern Recognition*, pages 8028–8038, 2020. 2, 6
- [41] J. Song, Chenlin Meng, and Stefano Ermon. Denoising diffusion implicit models. *International Conference on Learning Representations*, 2021. 2
- [42] Xiao Song, Guorun Yang, Xinge Zhu, Hui Zhou, Zhe Wang, and Jianping Shi. Adastereo: A simple and efficient approach for adaptive stereo matching. In *IEEE/CVF Conference on Computer Vision and Pattern Recognition*, pages 10328–10337, 2021. 3
- [43] Matthew Tancik, Pratul Srinivasan, Ben Mildenhall, Sara Fridovich-Keil, Nithin Raghavan, Utkarsh Singhal, Ravi Ramamoorthi, Jonathan Barron, and Ren Ng. Fourier features let networks learn high frequency functions in low dimensional domains. *Advances in neural information processing systems*, 33:7537–7547, 2020. 3
- [44] Joshua Tokarsky, Ibrahim Abdulhafiz, Satya Ayyalasomayajula, Mostafa Mohsen, Navya G. Rao, and Adam Forbes. PLT-D3: A High-fidelity Dynamic Driving Simulation Dataset for Stereo Depth and Scene Flow, 2024. 4
- [45] Alessio Tonioni, Matteo Poggi, Stefano Mattoccia, and Luigi Di Stefano. Unsupervised adaptation for deep stereo. In *IEEE International Conference on Computer Vision*, pages 1605–1613, 2017. 3
- [46] Alessio Tonioni, Matteo Poggi, Stefano Mattoccia, and Luigi Di Stefano. Unsupervised domain adaptation for depth prediction from images. *IEEE transactions on pattern analysis and machine intelligence*, 42(10):2396–2409, 2019. 3
- [47] Alessio Tonioni, Oscar Rahnama, Thomas Joy, Luigi Di Stefano, Thalaisyasingam Ajanthan, and Philip HS Torr. Learning to adapt for stereo. In *IEEE/CVF Conference on Computer Vision and Pattern Recognition*, pages 9661–9670, 2019. 3
- [48] Alessio Tonioni, Fabio Tosi, Matteo Poggi, Stefano Mattoccia, and Luigi Di Stefano. Real-time self-adaptive deep stereo. In *IEEE/CVF Conference on Computer Vision and Pattern Recognition*, pages 195–204, 2019. 3
- [49] Fabio Tosi, Yiyi Liao, Carolin Schmitt, and Andreas Geiger. Smd-nets: Stereo mixture density networks. In *IEEE/CVF Conference on Computer Vision and Pattern Recognition*, pages 8942–8952, 2021. 4
- [50] Fabio Tosi, Alessio Tonioni, Daniele De Gregorio, and Matteo Poggi. Nerf-supervised deep stereo. In *IEEE/CVF Conference on Computer Vision and Pattern Recognition*, pages 855–866, 2023. 2, 3, 8
- [51] Fabio Tosi, Luca Bartolomei, and Matteo Poggi. A survey on deep stereo matching in the twenties. *International Journal of Computer Vision*, 2025. 4
- [52] Jonathan Tremblay, Thang To, and Stan Birchfield. Falling things: A synthetic dataset for 3d object detection and pose

- estimation. In *IEEE Conference on Computer Vision and Pattern Recognition Workshops*, pages 2038–2041, 2018. 4
- [53] Hung-Yu Tseng, Qinbo Li, Changil Kim, Suhil Alsisan, Jia-Bin Huang, and Johannes Kopf. Consistent view synthesis with pose-guided diffusion models. In *IEEE/CVF Conference on Computer Vision and Pattern Recognition*, pages 16773–16783, 2023. 1
- [54] Igor Vasiljevic, Nick Kolkin, Shanyi Zhang, Ruotian Luo, Haochen Wang, Falcon Z. Dai, Andrea F. Daniele, Mohammadreza Mostajabi, Steven Basart, Matthew R. Walter, and Gregory Shakhnarovich. DIODE: A Dense Indoor and Outdoor D ϵ pth Dataset. *CoRR*, abs/1908.00463, 2019. 7
- [55] Lezhong Wang, Jeppe Revall Frisvad, Mark Bo Jensen, and Siavash Arjomand Bigdeli. Stereodiffusion: Training-free stereo image generation using latent diffusion models. In *IEEE/CVF Conference on Computer Vision and Pattern Recognition*, pages 7416–7425, 2024. 1, 2, 3, 5, 6, 7
- [56] Qiang Wang, Shizhen Zheng, Qingsong Yan, Fei Deng, Kaiyong Zhao, and Xiaowen Chu. Irs: A large naturalistic indoor robotics stereo dataset to train deep models for disparity and surface normal estimation. In *IEEE International Conference on Multimedia and Expo*, pages 1–6. IEEE, 2021. 1, 4
- [57] Wenshan Wang, DeLong Zhu, Xiangwei Wang, Yaoyu Hu, Yuheng Qiu, Chen Wang, Yafei Hu, Ashish Kapoor, and Sebastian Scherer. Tartanair: A dataset to push the limits of visual slam. In *IEEE/RSJ International Conference on Intelligent Robots and Systems*, pages 4909–4916. IEEE, 2020. 1, 4
- [58] Yang Wang, Peng Wang, Zhenheng Yang, Chenxu Luo, Yi Yang, and Wei Xu. Unos: Unified unsupervised optical-flow and stereo-depth estimation by watching videos. In *IEEE/CVF Conference on Computer Vision and Pattern Recognition*, pages 8071–8081, 2019. 3
- [59] Yuran Wang, Yingping Liang, Hesong Li, and Ying Fu. Mono2stereo: Monocular knowledge transfer for enhanced stereo matching. *arXiv preprint arXiv:2411.09151*, 2024. 3, 8
- [60] Jamie Watson, Oisín Mac Aodha, Daniyar Turmukhambetov, Gabriel J Brostow, and Michael Firman. Learning stereo from single images. In *European Conference on Computer Vision*, pages 722–740. Springer, 2020. 2, 3, 6, 7, 8
- [61] Zhexiao Xiong, Feng Qiao, Yu Zhang, and Nathan Jacobs. Stereoflowgan: Co-training for stereo and flow with unsupervised domain adaptation. In *34th British Machine Vision Conference 2023, BMVC 2023, Aberdeen, UK, November 20-24, 2023*. BMVA, 2023. 3
- [62] Gangwei Xu, Xianqi Wang, Zhaoxing Zhang, Junda Cheng, Chunyuan Liao, and Xin Yang. Igev++: Iterative multi-range geometry encoding volumes for stereo matching. *IEEE Transactions on Pattern Analysis and Machine Intelligence*, 2025. 7, 8
- [63] Zhongcong Xu, Jianfeng Zhang, Jun Hao Liew, Hanshu Yan, Jia-Wei Liu, Chenxu Zhang, Jiashi Feng, and Mike Zheng Shou. Magicanimate: Temporally consistent human image animation using diffusion model. In *IEEE/CVF Conference on Computer Vision and Pattern Recognition*, pages 1481–1490, 2024. 2
- [64] Lihe Yang, Bingyi Kang, Zilong Huang, Xiaogang Xu, Jiashi Feng, and Hengshuang Zhao. Depth anything: Unleashing the power of large-scale unlabeled data. In *IEEE/CVF Conference on Computer Vision and Pattern Recognition*, pages 10371–10381, 2024. 1, 4
- [65] Lihe Yang, Bingyi Kang, Zilong Huang, Zhen Zhao, Xiaogang Xu, Jiashi Feng, and Hengshuang Zhao. Depth anything v2. *Advances in Neural Information Processing Systems*, 37:21875–21911, 2024. 1, 7, 8
- [66] Lvmin Zhang, Anyi Rao, and Maneesh Agrawala. Adding conditional control to text-to-image diffusion models. In *IEEE/CVF International Conference on Computer Vision*, pages 3836–3847, 2023. 2
- [67] Yiran Zhong, Yuchao Dai, and Hongdong Li. Self-supervised learning for stereo matching with self-improving ability. *arXiv preprint arXiv:1709.00930*, 2017. 3
- [68] Bolei Zhou, Hang Zhao, Xavier Puig, Sanja Fidler, Adela Barriuso, and Antonio Torralba. Scene parsing through ade20k dataset. In *IEEE Conference on Computer Vision and Pattern Recognition*, pages 633–641, 2017. 7